JOURNAL OF Materials CHEMISTRY

The stannides LiAuSn and $LiAu_3Sn_4$: synthesis, structure and chemical bonding

Rolf-Dieter Hoffmann,[a] Dirk Johrendt,[b] Zhiyun Wu[a] and Rainer Pöttgen*[a]

[a]*Institut für Anorganische und Analytische Chemie und Sonderforschungsbereich 458, Westfälische Wilhelms-Universität Münster, Wilhelm-Klemm-Straße 8, D-48149 Münster, Germany. E-mail: pottgen@uni-muenster.de*

[b]*Institut für Anorganische Chemie und Strukturchemie II, Heinrich-Heine-Universität Düsseldorf, Universitätsstraße 1, D-40225 Düsseldorf, Germany. E-mail: johrendt@uni-duesseldorf.de*

Received 15th October 2001, Accepted 10th January 2002
First published as an Advance Article on the web 4th February 2002

The stannides LiAuSn and $LiAu_3Sn_4$ were synthesized from the elements by reaction in sealed tantalum tubes in a resistance furnace. LiAuSn crystallizes with a ZrBeSi type structure, space group $P6_3/mmc$: a = 467.08(8) pm, c = 603.7(1) pm, $wR2$ = 0.0403, 87 F^2 values, 7 variables. The gold and tin atoms form a planar network of condensed Au_3Sn_3 hexagons (270 pm Au–Sn) which are rotated by 60° around the c axis in every other layer. The lithium atoms are located between these layers. LiAuSn may be classified as a lithium intercalated heterographite according to $Li^+[AuSn]^-$. $LiAu_3Sn_4$ adopts a polar structure, space group $P6_3mc$, which has been refined for an inversion twin: a = 448.31(6) pm, c = 2055.7(4) pm, $wR2$ = 0.0814, BASF = 0.13(2), 699 F^2 values, 25 variables. This new structure type may be considered as an intergrowth of slightly distorted NiAs and $CaAl_2Si_2$ related slabs of compositions *AuSn* and *$LiAu_2Sn_2$*. Short (285 pm) Au–Au distances within the *AuSn* slab are indicative for significant Au–Au bonding. The lithium atoms fill tetrahedral voids formed by the gold atoms within the *$LiAu_2Sn_2$* slab. Chemical bonding analysis by TB-LMTO-ASA calculations confirm the covalently bonded $[AuSn]^-$ polyanion in LiAuSn. Each network atom participates in three two-electron two-center Au–Sn σ-bonds, whereas π-bonding is absent. The crystal orbital Hamilton populations (COHP) analysis of $LiAu_3Sn_4$ reveals almost equal Au–Sn bonding energies for the three Au atoms despite their different tin environments. Au–Au bonding in $LiAu_3Sn_4$ is strong and shows the same electronic features as in binary AuSn with NiAs structure.

Introduction

The ternary systems alkali metal–gold–tin have only scarcely been investigated in recent years.[1–13] So far the structures of the stannides Li_2AuSn,[1,2,4,8] LiMgAuSn,[8] NaAuSn,[3,5,10] $Na_xAu_ySn_z$,[7] Na_2AuSn_3,[13] A_3AuSn_4 (A = K, R, Cs),[12] KAu_4Sn_2[6] and $A_4Au_7Sn_2$ (A = Rb, Cs)[9,11] have been reported. According to temperature-dependent resistivity measurements K_3AuSn_4[12] and Na_2AuSn_3[13] are metallic conductors. The gold valence state in Li_2AuSn was investigated by ^{197}Au Mössbauer spectroscopy.[4] Furthermore Li_2AuSn was discussed as a prospective anode material for non-aqueous electrochemical cells.[14] In view of the promising properties of such lithium-based materials, we have recently started a more systematic investigation of the lithium–transition metal–tin systems resulting in the new stannides $LiTSn_4$ (T = Ru, Rh, Ir),[15] which show a small lithium mobility.[16] Herein we report on the synthesis, the crystal structures and a chemical bonding analysis of the lithium-based stannides LiAuSn and $LiAu_3Sn_4$. Excerpts of this work have been presented at a conference.[17]

Experimental

Starting materials for the preparation of LiAuSn and $LiAu_3Sn_4$ were lithium rods (Merck, >99%), gold wire (Degussa-Hüls, Ø 1 mm, >99.9%) and a tin bar (Heraeus, 99.9%). The lithium rods were cut into smaller pieces under dry paraffin oil and subsequently washed with *n*-hexane. The paraffin oil and *n*-hexane were dried over sodium wire. The lithium pieces were kept in Schlenk tubes under argon prior to the reactions. Argon was purified over titanium sponge (900 K), silica gel and molecular sieves.

The lithium pieces were mixed with the gold wire and pieces of the tin bar in the ideal 1 : 1 : 1 and 1 : 3 : 4 atomic ratios and sealed in tantalum ampoules (tube volume about 1 cm^3) under an argon pressure of about 800 mbar in an arc-melting apparatus.[18] The sealed tantalum tubes were subsequently enclosed in evacuated silica tubes to avoid oxidation and first rapidly heated at 1070 K, cooled to 870 K within 3 h and held at this temperature for 2 days. The tubes were finally quenched in air by radiative heat loss. The samples could readily be separated from the tubes. No reaction of the samples with the container material was observed. The two stannides are stable in air over several weeks. They are light grey in polycrystalline form. The single crystals exhibit metallic lustre.

The purity of the samples was checked by X-ray powder diffraction. $LiAu_3Sn_4$ was characterized through its Guinier powder pattern using Cu $K\alpha_1$ radiation and α-quartz (a = 491.30 pm, c = 540.46 pm) as an internal standard. The LiAuSn powder diagram was recorded on a Stoe StadiP diffractometer with Cu $K\alpha_1$ radiation and 5N silicon (a = 543.07 pm) as an external standard. The hexagonal lattice parameters (see Table 1) were obtained from least-squares fits of the powder data. The correct indexing of the patterns was ensured through intensity calculations[19] using the atomic positions of the structure refinements. In both cases the lattice parameters of the powders and the single crystals agreed well.

Irregularly shaped single crystals of both stannides were isolated from the crushed samples. They were examined by Laue photographs on a Buerger precession camera in order to establish their quality. Single crystal intensity data of $LiAu_3Sn_4$

 DOI: 10.1039/b109381a

Table 1 Crystal data and structure refinement for LiAuSn and $LiAu_3Sn_4$

Empirical formula	LiAuSn	$LiAu_3Sn_4$
Molar mass	322.60 g mol^{-1}	1072.60 g mol^{-1}
Lattice parameters (powder data)	a = 467.08(8) pm	a = 448.31(6) pm
	c = 603.7(1) pm	c = 2055.7(4) pm
	V = 0.1141 nm^3	V = 0.3578 nm^3
Crystal system	Hexagonal	Hexagonal
Space group	$P6_3/mmc$	$P6_3mc$
Formula units per cell	Z = 2	Z = 2
Calculated density	9.39 g cm^{-3}	9.96 g cm^{-3}
Crystal size	10 × 25 × 30 μm^3	25 × 30 × 60 μm^3
Transmission ratio (max./min.)	3.24	2.25
Absorption coefficient	74.7 mm^{-1}	74.9 mm^{-1}
F(000)	264	880
Detector distance	50 mm	—
Exposure time	8 min	—
φ range; increment	0–180°; 2.0°	—
Profile; pixel	13–23	—
θ range for data collection	5°–31°	3°–35°
Range in hkl	±6, ±6, ±8	±7, ±7, ±33
Total no. reflections	1122	5032
Independent reflections	87 (R_{int} = 0.0782)	699 (R_{int} = 0.0852)
Reflections with $I > 2\sigma(I)$	80 (R_{sigma} = 0.0322)	512 (R_{sigma} = 0.0407)
Data/parameters	87/7	699/25
Goodness-of-fit on F^2	1.228	1.185
Final R indices [$I > 2\sigma(I)$]	$R1$ = 0.0150	$R1$ = 0.0302
	$wR2$ = 0.0394	$wR2$ = 0.0635
R indices (all data)	$R1$ = 0.0186	$R1$ = 0.0605
	$wR2$ = 0.0403	$wR2$ = 0.0814
Extinction coefficient	0.027(2)	0.0070(4)
BASF	—	0.13(2)
Largest diff. peak and hole	0.92 and −1.09 e $Å^{-3}$	5.38 and −4.81 e $Å^{-3}$

were collected at room temperature by use of a four-circle diffractometer (CAD4) with graphite monochromatized Mo Kα radiation (71.073 pm) and a scintillation counter with pulse height discrimination. The scans were performed in the $\omega/2\theta$ mode. An empirical absorption correction was applied on the basis of Ψ-scan data. The LiAuSn crystal was investigated in the oscillation mode on a Stoe image plate system (IPDS) with graphite monochromatized Mo Kα radiation. A numerical absorption correction was applied to the data. All relevant crystallographic data and experimental details for the data collections are listed in Table 1.

Careful analyses of both data sets showed high hexagonal Laue symmetry $6/mmm$, and the systematic extinctions (hhl only observed with $l = 2n$, $00l$ only with $l = 2n$) led to the space groups $P6_3mc$, $P\bar{6}2c$, and $P6_3/mmc$. The centrosymmetric group $P6_3/mmc$ was found to be correct for LiAuSn, while $LiAu_3Sn_4$ crystallizes with the non-centrosymmetric group $P6_3mc$. The starting atomic positions were deduced from automatic interpretations of direct methods with SHELXS-97[20] and the two structures were successfully refined using SHELXL-97 (full-matrix least-squares on F_o^2)[21] with anisotropic atomic displacement parameters for the gold and tin sites. The lithium sites were clearly located from subsequent difference Fourier syntheses and these sites were refined with isotropic displacement parameters. For $LiAu_3Sn_4$ the displacement parameter was fixed at a value of 100 pm^2. The Flack parameter[22,23] of the non-centrosymmetric stannide $LiAu_3Sn_4$ indicated twinning by inversion. This was taken into account for in the final least-squares cycles where a batch scale factor of 0.13(2) was refined.

As a check for the correct composition, the occupancy parameters of the gold and tin sites were refined in a separate series of least-squares cycles. These sites were all fully occupied within two standard deviations and there were no indications for Au/Sn mixing. In the final cycles the ideal occupancy parameter were assumed again. Final difference Fourier syntheses revealed no significant residual peaks (see Table 1). The largest residual peaks were close to the metal sites and most likely resulted from insufficient absorption corrections of these strongly absorbing compounds. The positional parameters and interatomic distances are listed in Tables 2 and 3. Listings of the observed and calculated structure factors are available.†

Table 2 Atomic coordinates and isotropic displacement parameters (pm^2) for LiAuSn and $LiAu_3Sn_4$

Atom	Wyckoff site	x	y	z	U_{eq}[a]
LiAuSn (space group $P6_3/mmc$)					
Li	2a	0	0	0	222(63)
Au	2c	1/3	2/3	1/4	166(3)
Sn	2d	1/3	2/3	3/4	162(3)
$LiAu_3Sn_4$ (space group $P6_3mc$)					
Li	2b	1/3	2/3	0.211(3)	100[b]
Au1	2a	0	0	0.16473(9)	116(2)
Au2	2b	1/3	2/3	0.48426(9)	162(3)
Au3	2b	1/3	2/3	0.34576(6)	136(4)
Sn1	2b	2/3	1/3	0.1251(1)	109(5)
Sn2	2b	2/3	1/3	0.4082(2)	142(4)
Sn3	2a	0	0	0.0294(1)	159(7)
Sn4	2a	0	0	0.2958(1)	111(7)

[a] U_{eq} is defined as one third of the trace of the orthogonalized U_{ij} tensor. [b] Fixed parameter.

Self-consistent band structure calculations were performed using the LMTO-method in its scalar-relativistic version (program TB-LMTO-ASA).[24] Detailed descriptions are given elsewhere.[25,26] Reciprocal space integrations were performed with the tetrahedron method using 594 k points for LiAuSn and 222 k points for $LiAu_3Sn_4$ within the irreducible wedges of the Brillouin zones.[27] The basis sets consisted of 2s/2p/3d for Li, 6s/6p/5d/5f for Au and 5s/5p/5d/4f for Sn. The 2p/3d orbitals of Li, 5f of Au and 5d/4f of Sn were treated by the downfolding technique.[28] In order to achieve space filling within the atomic sphere approximation, interstitial spheres are introduced to avoid too large overlap of the atom-centered

†Details may be obtained from: Fachinformationszentrum Karlsruhe, D-76344 Eggenstein-Leopoldshafen (Germany), by quoting the Registry No's. CSD-412208 (LiAuSn) and CSD-412207 ($LiAu_3Sn_4$).

Table 3 Interatomic distances (pm) in the structures of LiAuSn and $LiAu_3Sn_4$, calculated with the atomic positions refined from the single crystal data and the lattice parameters taken from X-ray powder data (all distances within the first coordination sphere are listed)

LiAuSn										
Li	2	Li	301.9(1)	Au	3	Sn	269.7(1)	Sn	3	Au	269.7(1)
	6	Au	309.0(1)		2	Sn	301.9(1)		2	Au	301.9(1)
	6	Sn	309.0(1)		6	Li	309.0(1)		6	Li	309.0(1)
$LiAu_3Sn_4$										
Li	3	Au1	276(2)	Au3	1	Li	276(7)	Sn3	3	Au2	274.9(1)
	1	Au3	276(7)		3	Sn4	278.5(1)		1	Au1	278.3(3)
	3	Sn4	312(4)		1	Au2	284.7(2)		3	Sn1	325.2(2)
	3	Sn1	314(4)		3	Sn2	288.9(2)		3	Sn2	359.3(4)
Au1	1	Sn4	269.5(3)	Sn1	3	Au1	271.3(1)	Sn4	1	Au1	269.5(3)
	3	Sn1	271.3(1)		1	Au2	289.6(4)		3	Au3	278.5(1)
	3	Li	276(2)		3	Li	314(4)		3	Li	312(4)
	1	Sn3	278.3(3)		3	Sn3	325.2(2)		3	Sn2	346.9(4)
Au2	3	Sn3	274.9(1)	Sn2	3	Au3	288.9(2)				
	1	Au3	284.7(2)		3	Au2	302.4(2)				
	1	Sn1	289.6(4)		3	Sn4	346.9(4)				
	3	Sn2	302.4(2)		3	Sn3	359.3(4)				

spheres. The empty spheres positions and radii were calculated automatically. We did not allow overlaps of more than 15% for any two atom centered spheres. The COHP method was used for the bond analysis.[29] COHP gives the energy contributions of all electronic states for a selected bond. The values are negative for bonding and positive for antibonding interactions. With respect to the well known COOP diagrams, we plot −COHP(E) to get positive values for bonding states.

Results and discussion

The new stannides LiAuSn and $LiAu_3Sn_4$ were discovered in the ternary system lithium–gold–tin. So far only the lithium-rich stannide Li_2AuSn[1,2,4,8] with a face-centered cubic structure has been reported. Equiatomic LiAuSn (Fig. 1) crystallizes with a ZrBeSi type structure,[30,31] a superstructure of the well known AlB_2 type. The gold and tin atoms are ordered on the boron sites. The $[Au_3Sn_3]$ layers are rotated by 60° around the *c* axis in every other layer, leading to a doubling of the *c* axis with respect to the AlB_2 type. The refinement with anisotropic displacement parameters gave no hint for puckering of the $[Au_3Sn_3]$ layers. Within these layers, the Au–Sn distances of 270 pm are slightly smaller than the sum of the covalent radii[32] of 274 pm, indicating significant Au–Sn interactions. The layers are well separated from each other *via* the lithium atoms. Thus, each gold atom has three near tin neighbours at 270 pm and two further tin contacts at 302 pm. The lithium atoms are sandwiched by two $[Au_3Sn_3]$ hexagons. The Li–Au and Li–Sn distances of 309 pm are both significantly longer than the sums of the covalent radii (256 pm Li + Au and 262 pm Li + Sn).[32,33] We can thus assume strong Au–Sn bonding within the layers but weaker bonding of the lithium atoms to these layers.

In view of the electronegativity differences (Li 0.98, Au 2.54, Sn 1.96, on the Pauling scale[33]) lithium is by far the most electropositive component of LiAuSn. We can thus assume an electron transfer from lithium to the [AuSn] network. This is confirmed by our preliminary ^{7}Li NMR experiments which show a single signal for LiAuSn at room temperature at a chemical shift of $\delta = 9.3$ ppm with respect to LiCl. Electron counting can approximately be written as $Li^+[AuSn]^-$.

The shortest Li–Li contacts of 302 pm occur *via* the center of the $[Au_3Sn_3]$ hexagons. Even though they are 2 pm shorter than the distances in elemental lithium,[34] these contacts may not be considered as bonding in view of the highly ionic character of the lithium atoms.

A further question concerns the charge distribution within the [AuSn] network. Preliminary ^{119}Sn Mössbauer data for LiAuSn revealed a single signal at room temperature at an elevated isomer shift of 2.5(1) mm s^{-1}, indicating a relatively high electron density at the tin atoms. A similar trend in electron density was recently observed for the stannides $CaRhSn_2$ and $CaPdSn_2$[35] where a higher isomer shift (2.21(3) mm s^{-1}) and consequently a higher electron density was found for the palladium compound. Thus, the tin atoms carry some of the negative charge within the [AuSn] network. More detailed temperature dependent ^{119}Sn Mössbauer and ^{7}Li solid state NMR investigations for LiAuSn in view of a potential lithium mobility are currently in progress.

Besides the experimental evidence, chemical bonding in LiAuSn was investigated by LMTO band structure calculations. Total and partial density of states (DOS) plots of LiAuSn are shown in Fig. 2. No energy gap is discerned at the Fermi level E_F in agreement with the metallic character of the compound. The large peak around −4 to −6.5 eV arises mainly from gold 5d levels, whereas the states below −8 eV are essentially from tin 5s orbitals. Strong hybridization of gold, tin and, to a lesser extent, lithium orbitals over the entire energy range becomes evident in the partial DOS curves in Fig. 2.

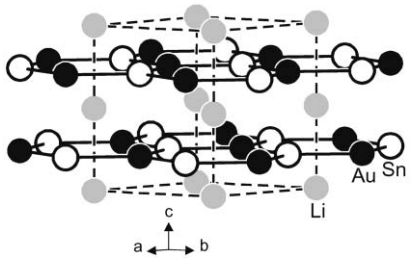

Fig. 1 Crystal structure of LiAuSn. The lithium, gold and tin atoms are drawn as grey, filled and open circles, respectively. The two-dimensionally infinite [AuSn] network is emphasized.

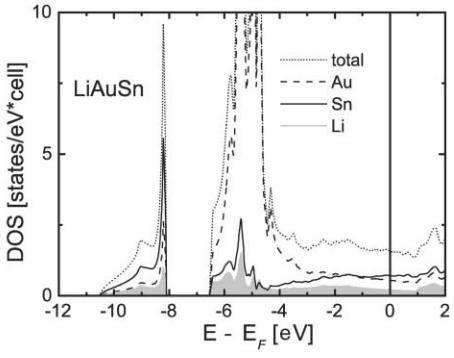

Fig. 2 Electronic DOS of LiAuSn. Dotted line, total DOS; broken line, Au partial DOS; solid line, Sn partial DOS; shaded region, Li partial DOS. The energy zero is taken at the Fermi level.

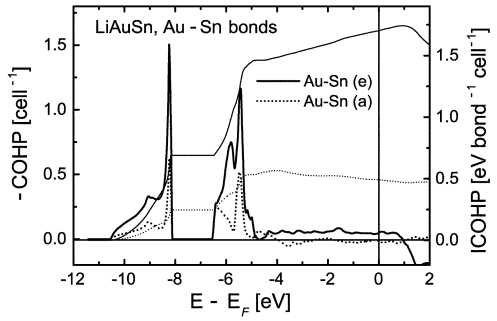

Fig. 3 COHP and their ICOHP of Au–Sn interactions in LiAuSn. Solid lines, Au–Sn bond within the Au_3Sn_3 hexagons; dotted lines, Au–Sn bond between the layers. Thin lines refer to the ICOHP scale (right).

In order to analyze the bonding situation in LiAuSn, we have calculated the COHPs of the equatorial (e) Au–Sn bonds within the hexagons and the axial (a) ones perpendicular to them, as depicted in Fig. 3. Exclusively bonding states are occupied up to the Fermi level. From the integrations of the COHP (ICOHP), we find the equatorial bonds to be almost four times stronger than the axial ones. The latter ones contribute merely 15% to the total Au–Sn bonding energy. The bonding states in the COHP plot coincide remarkably with the tin partial DOS of Fig. 2. This pattern is typical of covalent sp^2–σ-bonding between main group elements. The gold 5d levels seem not to contribute significantly to bonding, otherwise the COHP should be much higher between −5 and −6.5 eV. As expected for elements of the higher periods, we see no significant π-bonding levels in the COHP, which should otherwise appear between −5 eV and E_F. This bonding picture is consistent with the formulation $Li^+[AuSn]^-$. Six electrons are available out of the gold 5d shell to form three covalent Au–Sn bonds. Within the $[Au_3Sn_3]$ hexagons, gold is more electronegative than tin and carries therefore the main part of the charge transferred from lithium. This is in good agreement with the charge density distribution in Fig. 4. The (110)-plane clearly shows the covalent Au–Sn bonds, whose charge density is plainly shifted to gold. This is very similar to covalent bonds between main group elements of different electronegativities. In agreement with the COHP result, no distinct Au–Sn bonding is seen between the hexagonal $[Au_3Sn_3]$ layers in the charge density of Fig. 4. This emphasizes the layered, two-dimensional character of LiAuSn from the electronic structure viewpoint.

The second stannide, $LiAu_3Sn_4$, has a more complex crystal structure. It contains one lithium and three and four crystallographically independent gold and tin sites, respectively, as displayed in Fig. 5. Although this structure has a relatively long *c* axis, we can subdivide it into smaller slabs of known structures. As emphasized on the right-hand part of Fig. 5, the $LiAu_3Sn_4$ structure is built up from slightly distorted NiAs and $CaAl_2Si_2$[36] related slabs of compositions *AuSn* and $LiAu_2Sn_2$.

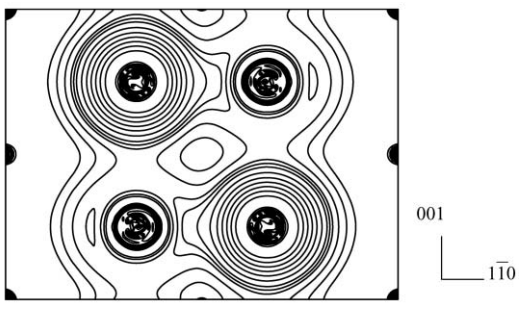

Fig. 4 Charge density distribution in the (110) plane of LiAuSn. Contour lines are shown on an exponential scale from 0.01 to 0.5 e^- au^{-3}.

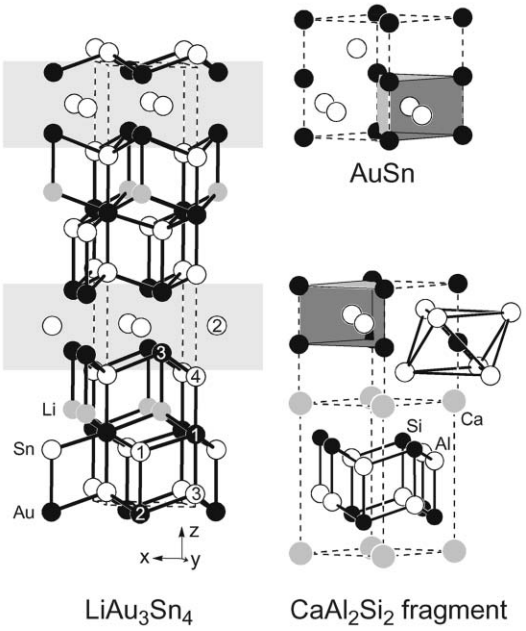

Fig. 5 Crystal structure of $LiAu_3Sn_4$ and its relation with the structures of AuSn (NiAs type) and $CaAl_2Si_2$. The NiAs related slabs are emphasized in the left-hand drawing by grey blocks. At the lower right-hand part we emphasize the stacking sequence of the NiAs and $CaAl_2Si_2$ related slabs. The lithium, gold and tin atoms are drawn as large grey, small filled and medium open circles, respectively. The crystallographically different sites are indicated. The Au–Au bonds are omitted for clarity in the drawing.

The Sn2 atoms within the NiAs slab have six gold neighbours in trigonal prismatic coordination at Sn–Au distances of 289 and 302 pm. The lattice parameters of this AuSn slab are $a' = 448$ pm and $c' = 285$ pm. At this point we should note that a binary stannide AuSn[37,38] with NiAs type structure with the lattice parameters $a = 432$ pm and $c = 552$ pm ($c/2 = 276$ pm) is known. The $c:a$ ratio of 0.639 for half the unit cell of binary AuSn is similar to $c':a' = 0.636$ for the AuSn slab in $LiAu_3Sn_4$. The overall distances in the AuSn slab of $LiAu_3Sn_4$, however, are larger: 276 pm Au–Au and 285 pm Au–Sn in binary AuSn as compared to 285 pm Au–Au and 270–302 pm Au–Sn in $LiAu_3Sn_4$. Thus, the AuSn slab has some flexibility and matches the electronic and geometric requirements of the other slab. The Au–Au distances in both slabs are smaller than in fcc gold[34] (288 pm).

The Au2 and Au3 atoms of the NiAs slab have a flattened distorted octahedral coordination of tin atoms with Au–Sn distances ranging from 275 to 302 pm as compared to 285 pm in binary AuSn. The Au2 atoms have one additional tin atom at 290 pm increasing the number of tin neighbours to 7. The shorter Au–Sn distances compare well with the sum of the covalent radii[32,33] of 274 pm. Within the NiAs related slab we observe no mirror plane. The lithium atoms are located in elongated tetrahedra formed by the Au1 and Au3 atoms. These tetrahedra point exclusively towards the $+c$ direction. This is the reason for the non-centrosymmetricity of the $LiAu_3Sn_4$ structure.

The shortest Sn–Sn distances of 325 pm occur between the Sn1 and Sn3 atoms. These compare well with the Sn–Sn distances in β-tin[34] (4 × 302 pm; 2 × 318 pm). Thus, besides strong Au–Au and Au–Sn interactions we observe also some weak Sn–Sn interactions in $LiAu_3Sn_4$.

The electronic structure of $LiAu_3Sn_4$ was calculated likewise by the LMTO method. We confine the discussion to the bonding interactions, because the DOS of $LiAu_3Sn_4$ is essentially of the same type as described above for LiAuSn. Gold is coordinated by five, six or seven tin atoms. In order to compare their bonding situation, we show the sums of the

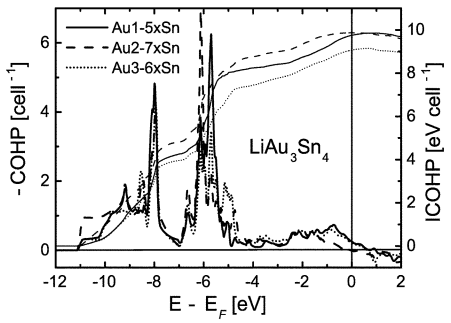

Fig. 6 COHP and their ICOHP of different Au–Sn interactions in $LiAu_3Sn_4$. Thin lines refer to the ICOHP scale (right).

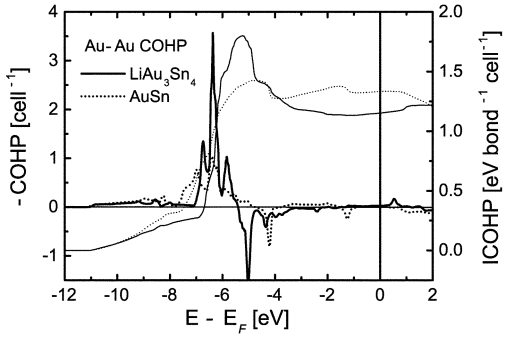

Fig. 7 COHP and their ICOHP of an Au–Au bond in $LiAu_3Sn_4$ (solid lines) and in binary AuSn (dotted lines). Thin lines refer to the ICOHP scale (right).

Au–Sn COHPs for Au1, Au2 and Au3 in Fig. 6. Again the bonding levels originate mainly by hybridization of Au 6s/6p with the tin 5s/5p orbitals and they are not much different for Au1, Au2 and Au3. Consequently, the total bonding energies (ICOHP) of the three gold sites are remarkably similar despite the different numbers of neighbours and geometries. In fact, the average calculated Au–Sn single bond energy of 1.6 eV $bond^{-1}$ in $LiAu_3Sn_4$ agrees well with the value of 1.7 eV $bond^{-1}$ in LiAuSn.

A special feature of $LiAu_3Sn_4$ is a short Au–Au distance at 285 pm, forming Au_2 dumbbells. Comparable Au–Au distances at 276 pm occur in binary AuSn as infinite chains. As we pointed out earlier, Au–Au bonding is strongly affected by the relativistic nature of gold, which leads to significant bonding energies despite a formal $5d^{10}$ configuration. We have calculated the COHP for one Au–Au bond in each structure (Fig. 7). The COHPs are very similar. Both plots show Au–Au bonding states around −6 eV and antibonding peaks at −5 and −4 eV for $LiAu_3Sn_4$ and AuSn, respectively. Due to weaker antibonding states, the ICOHP results in a slightly higher bonding energy for the binary compound, reflecting the slightly shorter Au–Au distance in AuSn as compared with $LiAu_3Sn_4$. However, the energy difference is only 15% and we can truly conclude that Au–Au bonding in $LiAu_3Sn_4$ is almost the same as in AuSn.

Acknowledgement

We are indebted to Dipl.-Ing. U. Ch. Rodewald and Dr. H. Piotrowski for the data collections and to the Degussa-Hüls AG for a generous gift of gold wire. This work was financially supported by the Deutsche Forschungsgemeinschaft (SFB 458: *Ionenbewegung in Materialien mit ungeordneten Strukturen – vom Elementarschritt zum makroskopischen Transport*) and the Fonds der Chemischen Industrie.

References

1 H. Pauly, A. Weiss and H. Witte, *Z. Metallkd.*, 1968, **59**, 47.
2 H.-U. Schuster, D. Thiedemann and H. Schönemann, *Z. Anorg. Allg. Chem.*, 1969, **370**, 160.
3 G. Wrobel and H.-U. Schuster, *Z. Naturforsch., B*, 1975, **30**, 806.
4 P. Gütlich, S. Odar and A. Weiss, *J. Phys. Chem. Solids*, 1976, **37**, 1011.
5 G. Wrobel and H.-U. Schuster, *Z. Anorg. Allg. Chem.*, 1977, **432**, 95.
6 H.-D. Sinnen and H.-U. Schuster, *Z. Naturforsch., B*, 1978, **33**, 1077.
7 W. Döring, W. Seelentag, W. Buchholz and H.-U. Schuster, *Z. Naturforsch., B*, 1979, **34**, 1715.
8 U. Eberz, W. Seelentag and H.-U. Schuster, *Z. Naturforsch., B*, 1980, **35**, 1341.
9 H.-D. Sinnen and H.-U. Schuster, *Z. Naturforsch., B*, 1981, **36**, 833.
10 G. Nuspl, K. Polborn, J. Evers, G. A. Landrum and R. Hoffmann, *Inorg. Chem.*, 1996, **35**, 6922.
11 U. Zachwieja and J. Wlodarski, *Z. Anorg. Allg. Chem.*, 1998, **624**, 1443.
12 U. Zachwieja, J. Müller and J. Wlodarski, *Z. Anorg. Allg. Chem.*, 1998, **624**, 853.
13 U. Zachwieja, *Z. Anorg. Allg. Chem.*, 2001, **627**, 353.
14 M. M. Thackeray, K. D. Kepler and J. T. Vaughey, Pat. No. WO 2000003443, Appl. No. WO 1999–US12868.
15 Zh. Wu, R.-D. Hoffmann and R. Pöttgen, *Z. Anorg. Allg. Chem.*, in press.
16 J. Senker, Zh. Wu, R.-D. Hoffmann, H. Trill, B. D. Mosel, H. Eckert and R. Pöttgen, unpublished results.
17 Zh. Wu, R.-D. Hoffmann, R. Pöttgen, R. Mishra, H. Eckert, F. M. Schappacher and H. Piotrowski, *Z. Kristallogr.*, 2001, **Suppl. 18**, 108.
18 R. Pöttgen, Th. Gulden and A. Simon, *GIT Labor-Fachzeitschrift*, 1999, **43**, 133.
19 K. Yvon, W. Jeitschko and E. Parthé, *J. Appl. Crystallogr*, 1977, **10**, 73.
20 G. M. Sheldrick, SHELXS-97, *Program for the Solution of Crystal Structures*, University of Göttingen, Germany, 1997.
21 G. M. Sheldrick, SHELXL-97, *Program for Crystal Structure Refinement*, University of Göttingen, Germany, 1997.
22 H. D. Flack and G. Bernadinelli, *Acta Crystallogr., A*, 1999, **55**, 908.
23 H. D. Flack and G. Bernadinelli, *J. Appl. Crystallogr.*, 2000, **33**, 1143.
24 O. K. Andersen and O. Jepsen, Tight-Binding LMTO Vers. 4.7, Max-Planck-Institut für Festkörperforschung, Stuttgart, 1994.
25 O. Jepsen, M. Snob and O. K. Andersen, L*inearized Band Structure Methods and its Applications*, Springer Lecture Notes, Springer-Verlag, Berlin, 1987.
26 H. L. Skriver, *The LMTO Method*, Springer-Verlag, Berlin, 1984.
27 O. K. Andersen and O. Jepsen, *Solid State Commun.*, 1971, **9**, 1763.
28 W. R. L. Lambrecht and O. K. Andersen, *Phys. Rev. B*, 1986, **34**, 2439.
29 R. Dronskowski and P. Blöchl, *J. Phys. Chem.*, 1993, **97**, 8617.
30 J. W. Nielsen and N. C. Baenziger, *Acta Crystallogr.*, 1954, **7**, 132.
31 R.-D. Hoffmann and R. Pöttgen, *Z. Kristallogr.*, 2001, **216**, 127.
32 L. Pauling, *The Nature of the Chemical Bond and the Structure of Molecules and Crystals*, Cornell University Press, Ithaca, NY, 1960.
33 J. Emsley, *The Elements*, Oxford University Press, Oxford, 1999.
34 J. Donohue, *The Structures of the Elements*, Wiley, New York, 1974.
35 R.-D. Hoffmann, D. Kußmann, U. Ch. Rodewald, R. Pöttgen, C. Rosenhahn and B. D. Mosel, *Z. Naturforsch., B*, 1999, **54**, 709.
36 E. I. Gladyshevskii, P. I. Kripyakevich and O. I. Bodak, *Ukr. Phys. J.*, 1967, **12**, 447.
37 J.-P. Jan, W. B. Pearson, A. Kjekshus and S. B. Woods, *Can. J. Phys.*, 1963, **41**, 2252.
38 J. S. Charlton, M. Cordey-Hayes and I. R. Harris, *J. Less-Common Met.*, 1970, **20**, 105.